



This is a repository copy of *ZnO nanopowder derived from brass ash: Sintering behavior and mechanical properties*.

White Rose Research Online URL for this paper:
<http://eprints.whiterose.ac.uk/101417/>

Version: Accepted Version

Article:

Lee, T-H., Nersisyan, H.H., Kwon, S-C. et al. (3 more authors) (2016) ZnO nanopowder derived from brass ash: Sintering behavior and mechanical properties. *International Journal of Mineral Processing*, 153. pp. 87-94. ISSN 0301-7516

<https://doi.org/10.1016/j.minpro.2016.05.007>

Article available under the terms of the CC-BY-NC-ND licence
(<https://creativecommons.org/licenses/by-nc-nd/4.0/>)

Reuse

This article is distributed under the terms of the Creative Commons Attribution-NonCommercial-NoDerivs (CC BY-NC-ND) licence. This licence only allows you to download this work and share it with others as long as you credit the authors, but you can't change the article in any way or use it commercially. More information and the full terms of the licence here: <https://creativecommons.org/licenses/>

Takedown

If you consider content in White Rose Research Online to be in breach of UK law, please notify us by emailing eprints@whiterose.ac.uk including the URL of the record and the reason for the withdrawal request.



eprints@whiterose.ac.uk
<https://eprints.whiterose.ac.uk/>

ZnO nanopowder derived from brass ash: sintering behavior and mechanical properties

Tae-Hyuk Lee^a, Hayk, H. Nersisyan^{a,b}, Suk-Cheol Kwon^a, Sin-Hyeong Joo^a,
Kyoung-Tae Park^c, Jong-Hyeon Lee^{a,b*}

^aGraduate School of Department of Materials Science & Engineering

^aRapidly Solidified Materials Research Center, Chungnam National University, 99
Daehak-ro, Yuseong-gu, Daejeon 34134, Republic of Korea

^cRare metal R&D Group, Korea Institute of Industrial Technology, , 7-47 Songdo-Dong,
Yeonsoo-Gu, Incheon 21999, Republic of Korea

*Corresponding author: Jong-Hyeon Lee

Type of article: regular paper

Address: Chungnam National University, Daejeon 305-764, South Korea

Phone: +82-42-821-6596

Fax: +82-42-822-5850

E-mail: jonglee@cnu.ac.kr

Abstract

The present investigation studied the recycling of zinc from brass ash which is a secondary product produced during the brass smelting process. A retiring cycle was devised to produce high-purity ZnO nanopowders. Recovery of more than 90 wt% of the total zinc available was achieved after the calcination of brass ash at 700 °C and a multistage hydrometallurgical treatment at room temperature. ZnO powder produced by the developed method was analyzed by X-ray diffraction, transmission electron scanning microscopy, ICP-AES and BET analysis. The ZnO nanopowder obtained from the brass ash was well dispersed and the size of the individual particles was in the range of 30–50 nm. The purity of the powder was 99.83 wt%, and the surface area was about 30.5 m²/g. A relative density level of about 98.1% was reached with ZnO pellets sintered at 1300 °C.

Keywords: Zinc oxide; Nanopowder; Brass ash; Calcination; Hydrometallurgical treatment.

1. Introduction

Zinc oxide is an important semiconductor with a relatively high excitation binding energy (60 meV) and a wide direct band gap (3.37 eV). The tailoring of this metal oxide to the desired shape has attracted extensive attention due to its various shape-induced functions. This high excitation binding energy allows excitonic transitions at room temperature, leading to high radiative recombination efficiency for spontaneous emission as well as a lower threshold voltage for emission. Zinc oxide nanoparticles (NPs) have received a considerable amount of attention due to their specific chemical, electrical, surface and microstructural properties. These nanoparticles with the advantages of a large volume-to-surface area ratio, high ultraviolet absorption, and a long life-span (Yu et al., 2004) have proved to have greater potential for use in gas sensors (Xu et al., 2000), solar cells (Yu et al., 2004), and photocatalyst degradation (Curri et al., 2003; Kamat et al., 2002) than TiO₂ NPs (Hong et al., 2005). They have also been employed as efficient catalysts for liquid phase hydrogenation (Hamminga et al., 2004), chemical absorption (Turton et al., 2004), and UV absorption in cosmetics and as an anti-virus agent (Hu et al., 2003). The physical and microstructural properties of ZnO can be modified by changing the synthetic method (Meulenkamp, 1998; Monticone et al., 1998).

For these reasons, the synthesis of ZnO nanoparticles is of great interest to researchers. Several chemical methods have been used in the synthesis of ZnO nanoparticles, such as sol-gel processing (Mondelaers et al., 2002; Tokumoto et al., 2003), mechanical milling (Damonte et al., 2004), homogeneous precipitation (Kim et al., 2005), spray pyrolysis (Okuyama and Lenggoro, 2003), organometallic synthesis (Kahn et al., 2005), thermal decomposition of organic precursors (Rataoul et al., 2002), supercritical water processing

(Viswanathan et al., 2003), RF plasma synthesis (Sato et al., 2003), direct precipitation (Wang and Gao, 2003), vapor transport processing (Yu et al., 2005), self-assembling (Koh et al., 2004), microemulsion synthesis (Singhai et al., 1997), microwave irradiation (Komarneni et al., 2000), hydrothermal processing (Zhang et al., 2004), thermal evaporation (Dai et al., 2003), mechanochemical synthesis (Ao et al., 2006), and wet chemical methods (Cao et al., 2006; Singh, 2010; Singh et al., 2009; Wang et al., 2004). Regarding these versatile applications and with various preparation methods in hand, the introduction of new and more facile synthetic routes based on the recycling of Zn-rich industrial brass ash is currently in great demand (Yeole et al., 2014). Because brass ash damages the environment, there are mainly four means of reusing brass ash: recycled smelting, vitrification, hydrometallurgy, and pyrometallurgy. In the past, the main research in this area focused on pyrometallurgy, and the main product of this method was zinc oxide containing chlorine, lead, and iron. This method is not effective and it has a number of disadvantages, such as the low purity of the recycled oxide, the excessive energy consumption required, and the production of dioxin when the materials are processed (Cheremisinoff, 2001). At present, hydrometallurgy is considered to be an effective and low-cost method for the recycling of industrial waste. For instance Rahman et al. (2013) prepared ZnO nanoparticles using galvanizing plant waste (zinc dross) containing 27.66% Zn. In their study, zinc dross was dissolved in an HCl solution and precipitated as Zn(OH)₂ upon the addition of ammonium hydroxide. A heat treatment at 500°C led to ZnO agglomerated particles, with a micrometer size powder with 97% purity obtained. ZnO nanopowders created from brass ash in the copper smelting industry were reported by Hsiao and Wang, (2011). This study used the multi-stage hydrometallurgical processing of the collected brass ash to recover valuable metals to form metal oxide

nanoparticles. ZnO nanoparticles were prepared by a reaction of a precursor with H₂SO₄ in aqueous solutions. Subsequently, a solution of appropriate metal-precursors was rapidly added to a NaOH solution under strong stirring. Upon the mixing of the two solutions, precipitates were immediately observed. The precipitates were washed with distilled water and then dried at room temperature. The average size of the individual ZnO particles was less than 100 nm, and the surface area was ~25 m²/g. However no purity data for ZnO was reported.

The aim of this work is to recover Zn from brass ash generated in the brass smelting industry (Seowon Co. Ltd.) in South Korea. A flow sheet is developed and tested to produce high purity ZnO nanoparticles. In this study, our observations of densification and grain growth in a temperature range from 900°C to 1300°C indicated good sinterability of the ZnO nanopowders derived from brass ash.

2. Experimental

2.1 Materials

The brass ash used in this study was obtained from Seowon Co. Ltd. In South Korea. The concentration of elements in the brass ash is shown in [Table 1](#). The content of ZnO is ~90 wt. % which corresponds to ~71.7 wt. % of Zn metal. The remaining 10 wt% is metal oxides (CuO, Al₂O₃, PbO, SiO₂, MnO, Fe₂O₃ and MgO) and carbon. The auxiliary chemicals used for the recycling of brass ash included concentrated sulfuric acid (H₂SO₄), Na₂CO₃ and Zn powder (particle size ≤45 μm). Also, polyvinylpyrrolidone (PVP) was used as a surfactant to control the size of the ZnO particles. All chemicals were purchased from Samchun Chemicals Co. Ltd., South Korea.

2.2. Brass ash processing technology

The processing of brass ash was carried out in three general steps: (i) roasting of the brass ash at 700°C in air to burn out carbon and eliminate easily volatile substances, (ii) multistage hydrothermal processing to produce the high-purity Zn-precipitate; and (iii) drying and thermal processing of the Zn- precipitate to produce the high-purity ZnO nanopowder.

The processing technology is shown in Fig. 1. In the first stage, approximately 100g of brass ash (Fig. 1a) was roasted in a laboratory box furnace at 700°C for 2 hours. After roasting, the weight of the brass ash was decreased to 97g and the color of the powder changed from light-black to brown (Fig. 1b) due to the burning of carbon. After cooling the roasted powder was transferred to a 2-liter glass beaker and mixed with 1.0 liter of distilled water while stirring at room temperature (Fig. 1c). Subsequently, approximately 120-130g of H₂SO₄ (98%) mixed with 500ml of water was slowly added to the brass ash. The amount of H₂SO₄ used in the experiment was slightly higher than the theoretically estimated amount (~110-115g) in order to realize the complete dissolution of ZnO and the other metal oxides, in the case CuO, Fe₂O₃ and MgO. After 30min of stirring, the brass ash was mostly dissolved and a cloudy suspension was obtained. The stirrer was turned off and the suspension was allowed to sit for a period of time (~30 min.), after which it was filtrated by a Buncher funnel using filter paper. As shown in Fig. 1d a sky-blue solution was obtained after the filtration step. The pH of the solution as measured by a pH meter (HI 8424, Romania) was approximately 2.7-3.0. The solid, which remained in the filter paper, was carefully rinsed with distilled water and dried in a laboratory oven for further characterization. The amount of solid that remained after the dissolution of the brass ash was about 5.0-5.3 g.

The as-produced sky-blue solution was then heated to 50°C on the magnetic heater, and approximately 1.0-2.0 g of the Zn powder preliminary dispersed in 50 ml water was poured

into the solution to reduce Cu and Fe metals from the corresponding sulfate salts (Fig. 1e). The solution was then stirred for 5-10min and the resultant brown color precipitate was separated from the solution rinsed with water, and then dried for further characterization. The amount of solid filtrate ranged from 1.1 to 1.3g. The as-purified solution (Fig. 1f) was then transferred to 5-liter glass beaker and close to 100g of Na₂CO₃ dissolved in 1.0 liter of water was slowly poured into the main solution, after which a white gel immediately formed (Fig. 1g). The gel was aged for 2 hours, filtered through a filter paper, rinsed with double-distilled water, and dried at 100°C for 12 hours. Using this method, 85g of the white powder obtained after drying (Fig. 1h). This was then heat-treated at 500°C for the thermal decomposition of the gel (Fig. 1i). The final yield of the ZnO nanoparticles from 100g of brass ash was about 75-80g, which is 90 wt.% of the total amount of Zn in the brass ash.

2.3 Analysis methods

The crystal structures and morphology of the brass ash and ZnO nanopowders were characterized by X-ray diffractometry with Cu K α radiation (Siemens D5000, Germany), field-emission scanning electron microscopy (FE-SEM, JEOL JSM-7000F) and transmission electron microscopy (TEM, JEOL JEM-1400, Japan). The compositions of the brass ash and the ZnO nanopowders were analyzed by ICP-AES (Perkin-Elmer, Optima 7300DV, U.S.A.) and by an automatic elemental analyzer (Thermo Scientific, Flash 2000, U.S.A.). The specific surface area of the samples was determined using an SA-9600 Brunauer–Emmett–Teller (BET) surface area analyzer (Horiba, USA). **The weight losses and heat flow of the starting brass ash during the calcination step were determined using a TGA N-1000, Scinco analyzer, South Korea.** The Raman scattering spectra were obtained at room temperature using a Horiba Jobin Yvon LABRAM-HR800 laser micro-Raman spectrometer with a 633 nm laser.

A Fourier-transform infrared spectroscopy (FTIR) analysis was conducted on a Biorad FTS-175C Fourier transform infrared spectra spectrometer.

2.4. Sintering

The ZnO nanopowder was pressed into 2~3 mm thick disc-shaped pellets with diameters of 20 mm at a pressure of 300 MPa. The pellets were sintered in a laboratory furnace at 900-1300°C in air for 2 h at a heating rate of 5°C/min. The as-sintered pellets were naturally cooled to room temperature in the furnace. The Archimedeian method was used to measure the densities of the sintered pellets, and the relative densities were calculated as a percentage of the measured density compared to the theoretical density. The grain size of the sintered pellets was estimated using image analysis software.

3. Results and discussion

3.1 Roasting of brass ash

An XRD analysis was performed to observe the phase composition of the brass ash and any possible changes that may have occurred due to the roasting at 700°C. The analysis results are shown in Fig. 2a. All of the peaks of the brass ash (Fig. 2a(i)) are in good agreement with the Wurtzite structure of ZnO. The sharper and higher peak intensities of the roasted sample imply that the latter has a larger crystallite size than the former (Fig. 2a(f)). Moreover, after roasting a trace amount of ZnAl_2O_4 phase was also found in the XRD patterns.

Figs. 2b and c show typical FE-SEM images of the brass ash before and after roasting. FE-SEM measurements show that the particles increase in size during the aging process; the

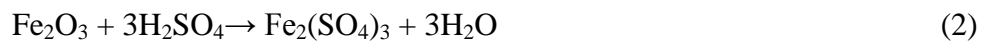
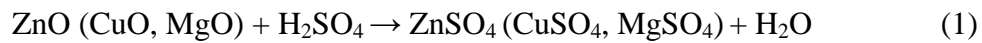
precipitated very fine powders (Fig. 2b) were removed after calcination leaving behind very uniform ZnO crystallites (Fig. 2c). These crystallites have a narrow size distribution and the average diameter of the particles as estimated from the micrograph ranges from 1 to 5 μm .

3.2. Hydrometallurgical processing of the roasted brass ash

The hydrometallurgical processing of the roasted brass ash involves the following two chemical steps: (i) leaching of the brass ash by a H_2SO_4 solution followed by purification of the leach liquor, and (ii) zinc extraction.

(i) Leaching and purification

ZnO and other metal oxides, such as CuO, Fe_2O_3 and MgO are readily soluble in H_2SO_4 at room temperature. Therefore, a liquor sample containing the corresponding metal sulfates was produced after the H_2SO_4 leaching procedure, as follows:

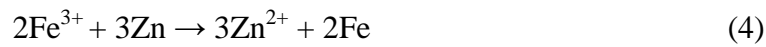


The solid residue that remains after the dissolution process was characterized by SEM-EDX and XRD analysis methods. The SEM micrograph shown in Fig. 3a reveals a polydisperse powder: the powder size is between 0.5 and 20 μm . According to the EDX analysis data shown in the inset of Fig. 3a, this powder consists of Al, Si, Zn, Pb, and O elements. Moreover, the XRD analysis of the solid residue revealed ZnAl_2O_4 as the main phase (Fig. 3b). More likely, the phases containing Pb, Si and Mn elements were not detected owing to their relatively low concentrations.

The purity of the liquor after the H_2SO_4 treatment was tested by an ICP analysis method. According to the analysis data the concentration of Mn in the liquor was approximately 80-

100 ppm. The concentration of other elements (Al, Zn, Pb, Si) were approximately 10-20 ppm.

The purification of the liquor from the Cu and Fe ions was subsequently performed with Zn powder, as described in the experimental section. During the reduction process the color of the liquor changed from sky-blue to transparent. The reduction of Cu and Fe ions to their metallic form occurred according to the following equations.



A SEM micrograph and the XRD patterns of the as-reduced powder are shown in Fig. 4. Two types of powders are shown in Fig. 4a: spherical powders 3-5 μm in diameter and small particles less than 0.5 μm in size. The spherical particles were identified by EDX as metallic Cu, and the smaller ones consisted of Cu, Fe, Zn, and O elements. It is believed that the metal powders reduced during the drying step become partially oxidized due to their small size. The XRD analysis clearly shows the peaks of the Cu metal; Zn and Fe peaks were not detected in the XRD analysis owing to their relatively low concentrations.

(ii) Zinc extraction

As described in section 2.2, the as-purified solution was then transferred to a 5-liter glass beaker, after which an amount of approximately 100 g of Na_2CO_3 dissolved in 1.0 liter of water was slowly poured into the main solution at room temperature for Zn precipitation. According to the XRD patterns shown in Fig. 5, the precipitate is mainly water-insoluble hydrozincite ($\text{Zn}_4\text{CO}_3(\text{OH})_6 \cdot \text{H}_2\text{O}$). Following the XRD data, the reaction between ZnSO_4 and Na_2CO_3 can be presented by the following equation:



The SEM analysis revealed plate-type fine particles of $\text{Zn}_4\text{CO}_3(\text{OH})_6\cdot\text{H}_2\text{O}$ (inset of Fig. 56). The thickness of the plates is less than 50 nm and the length ranges from 100 to 500 nm (inset in Fig. 5).

3.3 The synthesis and characterization of ZnO nanoparticles

Further calcination of $\text{Zn}_4\text{CO}_3(\text{OH})_6\cdot\text{H}_2\text{O}$ at 500°C in air produced ZnO nanoparticles according to the XRD patterns shown in Fig. 6. All peaks in the XRD patterns matched the ZnO hexagonal wurtzite structure. No peaks corresponding to Al_2O_3 , SiO_2 , or ZnAl_2O_4 were found in the XRD patterns. The peaks of ZnO are relatively wide; therefore the crystallite size (t) can be calculated using Scherrer's formula.

$$t = 0.9\lambda/\beta \cos \theta \quad (6)$$

where λ is the wavelength of the X rays used (1.54060 \AA), β is the full width at half maximum (FWHM) and θ is the angle of diffraction. The crystallite size of the ZnO powder as estimated by the Scherrer equation was approximately 40 nm.

To investigate the morphology, the ZnO nanopowder was dispersed in ethanol on a carbon-coated copper grid and high-resolution transmission electron microscopy (TEM) images (Fig. 7) were obtained at an accelerating voltage of 200 kV. The ZnO powders are round in shape and are well dispersed. The average size of the powders as estimated from Fig. 7a is between 30 and 50 nm. The selected-area electron diffraction (SAED) pattern (inset in Fig. 7a) has bright spots indicative of a polycrystalline nature with a symmetrical orientation of the ZnO nanoparticles in the sample. The crystallinity of the synthesized nanopowders is also supported by the bright-field TEM image shown in Fig. 7b. The ZnO powders show a spherical droplet shape, and the distances between the two lattice planes (d -spacing) were

found to be approximately 0.28 and 0.25 nm, corresponding to the d-spacing of the ZnO wurtzite structure in the (100) and (101) planar directions (Saoud et al., 2015).

The N₂ adsorption–desorption isotherms of the ZnO nanopowder recycled from the roasted brass ash are shown in Fig. 8a. The inset shows the pore-size distribution as determined by the Horvath--Kawazoe (HT) adsorption model. The adsorption isotherm of the ZnO sample exhibits the characteristics of a type-II isotherm (according to the IUPAC classification). The flatter region in the middle indicates the formation of a monolayer. At very low pressures, the micropores are filled with nitrogen gas. At the knee, the monolayer formation begins, and multilayer formation only occurs under medium pressure. At high pressures, capillary condensation occurs. Generally, type-II isotherms are usually associated with non-porous and macroporous materials, allowing unrestricted monolayer–multilayer adsorption to occur at high relative pressure (P/P_0) values (Rouquerol et al., 2013). The specific surface area (S), monolayer capacity (V_m), adsorbed gas quantity (V_p), Brunauer–Emmett–Teller (BET) constant (C), and average pore diameter (d_p) as determined from the BET analysis of the isotherms are given in Table 2. The specific surface of the ZnO sample was 30.484 m²/g. The monolayer capacity (V_m) of the sample was 6.774 cm³/g, the average pore diameter calculated from the BET plot (capillary condensation part) was 13.7 nm, and the BET constant was 173.63. The pore size distributions of the samples estimated from the HK plot (inset in Fig. 8a) range from 0.5 to 1.0 nm. Fig. 8b shows the room-temperature Raman spectrum of the ZnO nanoparticles, which is dominated by an intense and sharp peak at 438.92 cm⁻¹ assigned to the E_{2 (high)} mode, a characteristic feature of a wurtzite lattice. The other first-order Raman features for ZnO were observed at 580.49 cm⁻¹ corresponding to the A_{1 (LO)} mode. The next feature observed at 330.62 cm⁻¹ is assigned to second-order scattering (E_{2high} - E_{2low}) which

arises due to the overtones or combinations of first order modes (Cusco et al., 2007). Sequentially the absence of extra peaks from the impurities or host lattice defects could be regarded as vital for the fabricated nanoparticles to be phase pure and perfectly crystallized. Fig. 8c shows the FT-IR spectrum of the ZnO nanopowder. The band located near 466.15 cm^{-1} can be attributed to the Zn-O stretching mode. The band at 3466 cm^{-1} corresponds to the stretching vibration of O-H (H-bonded) and that at 1467.8 cm^{-1} was assigned to the first overtone of the fundamental stretching mode of O-H. These stretching vibrations correspond to water molecules bound on the surface of the sample. The band at 1119 cm^{-1} with a strong and sharp peak is attributed to the C-O stretching vibration.

The purity of the recycled ZnO nanopowder was also analyzed by the ICP-AES technique. These results are shown in Table 3. Here, two samples are shown in Table 3, ZnO-1 and ZnO-2. ZnO-1 was directly prepared from brass ash in the condition it was in when purchased from Seowon Co. Ltd. The ZnO-2 sample was prepared from brass ash calcined at $700\text{ }^{\circ}\text{C}$. The ZnO sample recycled from the calcined powder was 99.83 wt% pure, whereas only 98.5 wt% purity ZnO could be obtained from the raw brass ash powder. The calcination operation very effectively converted the metal oxides (e.g., Al_2O_3 , SiO_2 , PbO , MnO .) into low-solubility metal silicates, in this case Zn_2SiO_4 , Mn_2SiO_4 , Al_2O_3 , and SiO_2 . Our calculations also indicate that the yield of ZnO nanoparticles from the brass ash is high, at 90% to 95 wt%. The proposed method may therefore be useful to if used reduce the burden on the environment from electric arc furnace dust, the reduce the cost of ZnO nanopowders, and to extend the fields of application of these materials.

3.4. Properties of the sintered ZnO pellets

For the sintering procedure, 20g of ZnO powder was mixed with an aqueous solution

containing 0.6g of polyvinylpyrrolidone (PVP) using a twin screw kneader. After drying the mixture at 100°C, it was cold compacted into 2.0 mm thick cylindrical pellets 20 mm in diameter and then sintered at 900°C ~ 1300°C in air for 2 h. The relative density of the green pellets was 85.3%. The surface morphologies of the specimens sintered at different temperatures are compared in Fig. 9. Fig. 9a is a typical micrograph of grains freshly grown during the initial sintering stage, showing therefore a relatively low density (91.75%). From Fig. 9b, it is clear that the grain growth process began when the sintering temperature was increased to 1100°C. However, the porosity of the pellets remains high and the grain growth process remains unfinished. At 1200°C the size of the pores was sufficiently decreased and the grain size was increased above 2-10 μm (Fig. 9c). During the final stage of sintering, when the temperature reached to 1300°C, a perfectly bonded grain structure was obtained. The size of final grains was between 3 and 18 μm , as estimated from the micrograph (Fig. 9d). No secondary phases were noted at the grain junctions, indicating the high purity of the sintered pellets.

Fig. 10a shows a plot of the relative density as a function of the sintering temperatures. As expected, the densities of the sintered pellets increased with an increase the sintering temperature. The densification curve (Fig. 10a) exhibits a weaker increasing tendency with an increase in the temperature from 900 to 1200°C. Within the specified temperature range the relative density of the pellets was increased from 91.75 to 97.6%. A relative density of 98.1 % was measured after sintering at 1300°C for 2 h.

The effect of the sintering temperature on the Vickers microhardness (H_v) of the ZnO pellets is shown in Fig. 10b. The microhardness increased from 30.2 to 312.2 H_v as the sintering temperature increased from 900 to 1300°C due to the increase in the relative density

as shown in Fig. 10a. A maximum hardness value of 312.2H_v was obtained from the sample sintered at 1300°C. When compared to the micro hardness data reported by Mukhopadhyay et al. (2001) (~50-175H_v), it appeared that our ZnO samples were harder by nearly 1.7 times. This may have resulted from the high purity and the perfectly bonded grain structure.

4. Conclusions

A versatile process was developed to synthesize high purity ZnO nanopowders from brass ash, a by-product of the brass smelting industry. The processing of brass ash was performed in three steps: (i) roasting of brass ash at 700°C in air, (ii) hydrothermal processing for Zn purification and separation from the liquor; and (iii) drying and thermal processing of the solid precipitate to produce high-purity ZnO. An ICP-AES analysis revealed that the preliminary roasting of brass ash at 700°C may decrease the concentrations of Al, Pb, Si, and Mn metals in the final ZnO nanopowders. With regard to Cu and Fe metals, they were successfully eliminated by the intermediate processing of the brass ash solution with Zn powder. Therefore, after the processing of the as-purified ZnSO₄ solution by Na₂CO₃, a high-purity Zn₄CO₃(OH)₆·H₂O powder was precipitated. Further roasting of Zn₄CO₃(OH)₆·H₂O phase at 500°C resulted in a well-dispersed ZnO nanopowder whose size he was in the range of 30–50 nm. The purity of the powder was 99.83wt%, and the surface area was approximately 30.5 m²/g. Moreover, after sintering at 1300°C, the relative density and hardness of the sintered ZnO were 98.1% and 312.2H_v, respectively.

Acknowledgement

This research was supported by a grant from the Fundamental R&D Program for Energy

(No. 2012T100100092, (“Development of pyrometallurgical technology for low-quality urban mining by-products”) funded by the Ministry of Knowledge Economy, Republic of Korea.

References

- Ao, W., Li, J., Yang, H., Zeng, X., Ma, X., 2006. Mechanochemical synthesis of zinc oxide nanocrystalline. *Powder Technol.* 168 (3), 148-151.
- Cao, H.L., Qian, X.F., Gong, Q., Du, W.M., Ma, X.D., Zhu, Z.K., 2006. Shape- and size controlled synthesis of nanometer ZnO from a simple solution route at room temperature. *Nanotechnology* 17 (15), 3632-3636.
- Cheremisinoff P.N., 2001. *Handbook of pollution prevention practices*, CRC Press, Boca Raton.
- Curri, M.L., Comparelli, R., Cozzoli, P.D., Mascolo, G., Agostiano, A., 2003. Colloidal oxide nanoparticles for the photocatalytic degradation of organic dye. *Mater. Sci. Eng. C* 23 (1-2), 285-289.
- Cusco, R., Alarcon-Llado, E., Ibanez, J., Artus, L., Jimenez, J., Wang, B.G., Callahan, M.J., 2007. Temperature dependence of Raman scattering in ZnO. *Phys. Rev. B* 75, 165202.
- Dai, Z.R., Pan, Z.W., Wang, Z.L., 2003. Novel nanostructures of functional oxides synthesized by thermal evaporation. *Adv. Funct. Mater.* 13 (1), 9-24.
- Damonte, L.C., Mendoza Zelis, L.A., Mari Soucase, B., Hernandez Fenollosa M.A., 2004. Nanoparticles of ZnO obtained by mechanical milling. *Powder Technol.* 148 (1), 15-19.
- Hamminga, G.M., Mul, G., Mouljin, J.A., 2004. Real-time in situ ATR-FTIR analysis of the liquid phase hydrogenation of γ -butyrolactone over Cu-ZnO catalysts: a mechanistic

- study by varying lactone ring size. *Chem. Eng. Sci.* 59 (22-23), 5479-5485.
- Hong, R., Ren, Z., Ding, J., Li, H., 2005. Experimental investigation and particle dynamic simulation for synthesizing titania nanoparticles using diffusion flame. *Chem. Eng. J.* 108 (3), 203-212.
- Hsiao, L.Y., Wang, W.L., 2011. High-purity ZnO nanoparticles from fly ash in copper smelting industry and its application as additive agent in alkaline electrolyte. Abstract, 121, 220th ECS Meeting, 2011 The Electrochemical Society.
- Hu, Z., Oskam, G., Searson, P.C., 2003. Influence of solvent on the growth of ZnO nanoparticles. *J. Colloid Interface Sci.* 263 (2), 454-460.
- Kahn, M.L., Monge, M., Colliere, V., Senocq, F., Maisonnat, A., Chaudret, B., 2005. Size and shape control of crystalline zinc oxide nanoparticles: a new organometallic synthetic method. *Adv. Funct. Mater.* 15 (3), 458-468.
- Kamat, V.P., Huehn, R., Nicolaescu, R., 2002. A “sense and shoot” approach for photocatalytic degradation of organic contaminants in water. *J. Phys. Chem. B* 106 (4), 788-794.
- Kim, J.H., Choi, W.C., Kim, H.Y., Kang, Y., Park, Y.K., 2005. Preparation of mono-dispersed mixed metal oxide micro hollow spheres by homogeneous precipitation in a micro precipitator. *Powder Technol.* 153 (3), 166-175.
- Koh, Y.W., Lin, M., Tan, C.K., Foo, Y.L., Loh, K.P., 2004. Self-assembly and selected area growth of zinc oxide nanorods on any surface promoted by an aluminum precoat. *J. Phys. Chem. B* 108 (31), 11419–11425.
- Komarneni, S., Bruno, M., Mariani, E., 2000. Synthesis of ZnO with and without microwaves. *Mater. Res. Bull.* 35 (11), 1843-1847.

- Meulenkamp, E.A., 1998. Synthesis and growth of ZnO nanoparticles. *J. Phys. Chem. B* 102 (29), 5566-5572.
- Mukhopadhyay, A.K., Chaudhuri, M.R., Seal, A., Dalui, S.K., Banerjee, M., Phani, K.K., 2001. Mechanical characterization of microwave sintered zinc oxide. *Bull. Mater. Sci.* 24(2), 125-128.
- Mondelaers, D., Vanhoyland, G., Van den Rul, H., D'Haen, J., Van Bael, M.K., Mullens, J., Van Poucke, L.C., 2002. Synthesis of ZnO nanopowder via an aqueous acetate–citrate gelation method. *Mater. Res. Bull.* 37 (5), 901-914.
- Monticone, S., Tufeu, R., Kanaev, A.V., 1998. Complex nature of the UV and visible fluorescence of colloidal ZnO nanoparticles. *J. Phys. Chem. B* 102 (16), 2854-2862.
- Okuyama, K., Lenggoro, W.I., 2003. Preparation of nanoparticles via spray route. *Chem. Eng. Sci.* 58 (3-6), 537-547.
- Rahman, M.M, Qadir, M.R., Tahuran Neger, A.J.M., Kurny, A.S.W., 2013. Studies on the Preparation of Zinc Oxide from Galvanizing Plant Waste. *Am. J. Mater. Eng. and Tech.* 1(4), 59-64.
- Rataboul, F., Nayral, C., Casanove, M.J., Maisonnat, A., Chaudret, B., 2002. Synthesis and characterization of monodisperse zinc and zinc oxide nanoparticles from the organometallic precursor $[Zn(C_6H_{11})_2]$. *J. Organomet. Chem.* 643–644, 307-312.
- Rice, R.W., Wu, C.C., Borchelt, F., 1994. Hardness-grain-size relations in ceramics. *J. Am. Ceram. Soc.* 77(10), 2539-2553.
- Rouquerol, J., Rouquerol, F., Liewellyn, P., Maurin, G., Sing, K., 2013. Adsorption by powders and porous solids: principles, methodology and applications. second ed. Academic Press, San Diego

- Saoud, K., Alsoubaihi, R., Bensalah, N., Bora, T., Bertino, M., Dutta, J., 2015. Synthesis of supported silver nano-spheres on zinc oxide nanorods for visible light photocatalytic applications. *Mater. Res. Bull.* 63, 134-140.
- Sato, T., Tanigaki, T., Suzuki, H., Saito, Y., Kido, O., Kimura, Y., Kaito, C., Takeda, A., Kaneko, S., 2003. Structure and optical spectrum of ZnO nanoparticles produced in RF plasma. *J. Cryst. Growth* 255 (3-4), 313-316.
- Singh, A.K., 2010. Synthesis characterization electrical and sensing properties of ZnO nanoparticles. *Adv. Powder Technol.* 21 (6), 609-613.
- Singh, A.K., Viswanath, V., Janu, V.C., 2009. Synthesis, effect of capping agents, structural, optical and photoluminescence properties of ZnO nanoparticles. *J. Lumin.* 129 (8), 874-878.
- Singhai, M., Chhabra, V., Kang, P., Shah, D.O., 1997. Synthesis of ZnO nanoparticles for varistors application using Zn-substituted aerosol of microemulsion. *Mater.Res. Bull.* 32 (2), 239-247.
- Tokumoto, M.S., Briois, V., Santilli, C.V., Pulcinelli, S.H., 2003. Preparation of ZnO nanoparticles: structural study of the molecular precursor. *J. Sol–Gel Sci. Technol.* 26 (1-3), 547-551.
- Turton, R., Berry, D.A., Gardner, T.H., Miltz, A., 2004. Evaluation of zinc oxide sorbents in a pilot-scale transport reactor: sulfidation kinetics and reactor modeling. *Ind. Eng. Chem. Res.* 43 (5), 1235-1243.
- Viswanathan, R., Lilly, G.D., Gale, W.F., Gupta, R.B., 2003. Formation of zinc oxide-titanium dioxide composite nanoparticles in supercritical water. *Ind.Eng. Chem. Res.* 42 (22), 5535-5540.

- Wang, J., Gao, L., 2003. Synthesis, characterization of ZnO nanoparticles assembled in one-dimensional order. *Inorg. Chem. Commun.* 6 (7), 877-881.
- Wang, Z., Qian, X.F., Yin, J., Zhu, Z.K., 2004. Large-scale fabrication of tower-like, flowerlike, and tube-like ZnO arrays by a simple chemical solution route. *Langmuir* 20 (8), 3441–3448.
- Xu, J., Pan, Q., Shun, Y., Tian, Z., 2000. Grain size control and gas sensing properties of ZnO gas sensor. *Sens. Actuators B* 66 (1-3), 277-279.
- Yeole, K., Kadam, P., Mhaske, S., 2014. Synthesis and characterization of fly ash-zinc oxide nanocomposite. *J. Mater. Res. Technol.* 3(2) 186-190.
- Yu, D., Cai, R., Liu, Z., 2004. Studies on the photodegradation of Rhodamine dyes on nanometer-sized zinc oxide. *Spectrochim. Acta Part A* 60 (7), 1617-1624.
- Yu, W., Li, X., Gao, X., 2005. Catalytic Synthesis, structural characteristics of high-quality tetrapod-like ZnO nanocrystals by a modified vapor transport process. *Cryst. Growth Des.* 5 (1) 151-155.
- Zhang, H., Yang, D., Ji, Y., Ma, X., Xu, J., Que, D., 2004. Low temperature synthesis of flowerlike ZnO nanostructures by cetyltrimethyl ammonium bromide-assisted hydrothermal process. *J. Phys. Chem. B* 108 (13), 3955-3958.

List of Captions

Fig.1. Brass ash processing technology: a) brass ash; b) brass ash after calcination; c) water solution of the as-calcined brass ash; d) after dissolution in H_2SO_4 and filtration; e) Zn reduction and precipitate formation; f) filtered solution; g) solution treated by Na_2CO_3 ; h) the Zn-containing powder extracted from the solution i) powder calcined at $500^\circ C$ in air .

Fig.2. a) XRD patterns of brass ash before (i) and after roasting (f); b) SEM image of brass ash; c) SEM image of the roasted powder.

Fig. 3. a) SEM micrograph and EDX result; b) XRD patterns of the solid residue remaining after the dissolution process.

Fig. 4. a) SEM micrograph and EDX result; b) XRD patterns of the as-reduced powder.

Fig. 5. XRD patterns of $Zn_4CO_3(OH)_6 \cdot H_2O$ precipitated from the liquor by Na_2CO_3 . The inset is a SEM image of the precipitate.

Fig. 6. XRD patterns of ZnO nanopowder extracted from brass ash.

Fig. 7. TEM image of ZnO nanopowder: a) Bright field image (inset SAED pattern); b) High resolution image.

Fig. 8. a) Adsorption-desorption isotherms; b) Raman spectra; and c) FT-IR spectrum of ZnO nanopowders.

Fig. 9. SEM micrographs of ZnO pellets sintered for 2 h at: a) $1000^\circ C$; b) $1100^\circ C$; c) $1200^\circ C$; d) $1300^\circ C$

Fig. 10. a) Densification behavior and b) Vickers hardness of ZnO pellets sintered for 2 h at various temperatures.

Table 1. Chemical composition of the brass ash (wt.%)

Table 2. BET analysis results of the final ZnO powders.

Table 3. Chemical compositions of the final ZnO powders (wt %).